Polymer Journal (2019) 51:237–245
https://doi.org/10.1038/s41428-018-0150-7

ORIGINAL ARTICLE

Isothermal crystallization of poly(glycolic acid) studied by terahertz and infrared spectroscopy and SAXS/WAXD simultaneous measurements

Fumita Nishimura[1] · Hiromichi Hoshina[2] · Yukihiro Ozaki[1,3] · Harumi Sato[1]

Received: 20 August 2018 / Revised: 29 September 2018 / Accepted: 15 October 2018 / Published online: 16 November 2018

Abstract

Isothermal crystallization of poly(glycolic acid) (PGA) has been studied using terahertz (THz) and infrared (IR) spectroscopy and simultaneous small-angle X-ray scattering (SAXS)/wide-angle X-ray diffraction (WAXD) measurements. Changes in the intermolecular interactions in PGA during the isothermal crystallization were monitored using THz spectroscopy, which is an efficient technique for analyzing the higher-order structure of polymers. In the THz spectra, the temporal difference in the intensity observed in the isothermal crystallization is due to the difference in the vibrational origins of two bands at 192 and 65 cm^{-1}. The band at 192 cm^{-1} primarily originates from the intramolecular vibrational mode (twisting of the local structure of the PGA molecular chain). Furthermore, the band at 65 cm^{-1} exists due to the intermolecular vibration mode (C = O···H-C hydrogen bonds between polymer chains). In addition, these THz bands appeared after the appearance of the SAXS and WAXD peaks. When a lamellar structure is formed and the molecular chains are oriented, the THz band originating from the intermolecular vibration is observed. It is highly possible that the intermolecular vibration appearing in the THz spectra requires the molecular chains to be oriented.

Introduction

Poly(glycolic acid) (PGA) belongs to a family of synthetic biodegradable polyesters with high strength and low gas permeability (Fig. 1a)[1–8]. The crystalline structure of PGA has an orthorhombic system, $Pcmn - D_{2h}^{16}$ (with $a = 5.22$Å, $b = 6.19$ Å, and $c = 7.02$ Å) [3]. It is noteworthy that PGA shows the highest melting point (ca. 220 °C) among aliphatic polyesters. Chatani et al. [3]. reported that the short distance between the polymer chains estimated via X-ray crystallography of the ester groups results in a very high melting temperature and stabilizes the crystalline lattice.

Our group reported that PGA has weak hydrogen bonding between the H atom of the CH_2 group and the O atom of the -C-O-C- group in the crystalline structure based on analysis using infrared (IR) and Raman spectroscopy, wide-angle X-ray diffraction (WAXD), differential scanning calorimetry (DSC), quantum chemical calculations, and natural bond orbital (NBO) calculations [9]. The temperature-dependent variations of the CH_2 antisymmetric and symmetric stretching mode and the C-O-C stretching modes of PGA demonstrated gradually decreasing wavenumber shifts with temperature, while that of the C = O stretching band demonstrated a small shift [9]. Furthermore, some knowledge can be gained from quantum chemical calculations and temperature-dependent WAXD measurements regarding the high wavenumber shifts for the CH_2 antisymmetric and symmetric stretching modes and the C-O-C stretching mode of PGA due to intermolecular interactions along the (110) direction [9]. Moreover, the NBO calculations indicated that the stabilization energy for the

✉ Harumi Sato
hsato@tiger.kobe-u.ac.jp

[1] Graduate School of Human Development and Environment, Kobe University, Tsurukabuto3-11 Nada, Kobe 657-8501, Japan

[2] RIKEN Center for Advanced Photonics, 519-1399 Aramaki-Aoba, Aoba-ku, Sendai, Miyagi 980-0845, Japan

[3] Department of Chemistry, School of Science and Technology Kwansei Gakuin Univ, 2-1 Gakuen, Sanda, Hyogo 669-1337, Japan

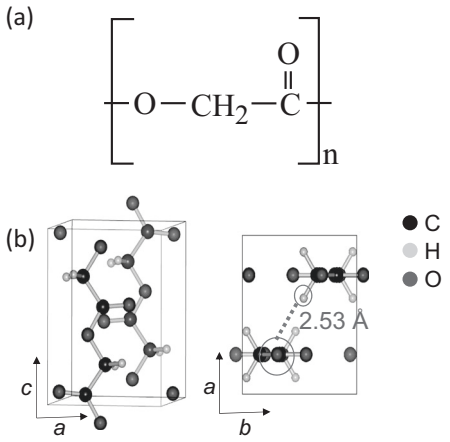

Fig. 1 **a** Chemical structure of PGA and **b** weak C-H···O (ether) hydrogen bonding in crystalline PGA

donor-acceptor interactions between the lone pair electron of the ether oxygen atom and the σ* bonding orbital of the C-H bond is considerably larger than that for the interactions between other orbitals, which is approximately 1 kcal mol^{-1} or weaker [9]. All the experimental and theoretical calculation results indicated a weakening of the C-H···O (ether) hydrogen bonding with increasing temperature (Fig. 1b) [9]. It is possible that the intermolecular interactions affect the higher-order structure of PGA, resulting in the unusually high melting point. The absorption peaks observed in the terahertz (THz) region originate from the higher-order structure, crystalline structure, and intermolecular interactions. Therefore, THz spectroscopy is a unique technique for analyzing higher-order conformations and intermolecular interactions in semicrystalline polymers such as PGA, poly-(R)-3-hydroxybutyrate (PHB), and polylactic acid (PLA) [10–19].

Two-dimensional correlation spectroscopy (2D-COS), proposed by Noda more than 25 years ago [20–22], has become an efficient technique for examining small spectral changes induced by an external perturbation. Guo et al. [23]. proposed a multistep crystallization process based on the 2D-COS analysis of small-angle X-ray scattering (SAXS) and WAXD profiles obtained during the isothermal crystallization of PHB. Recently, Hoshina et al. [13]. successfully investigated the temporal changes in the intensity of THz spectra obtained for PHB via 2D-COS analysis. Their study also demonstrated that 2D-COS for SAXS, WAXD, and THz spectra is an efficient technique for analyzing structural variations during polymer crystallization.

In this study, we have investigated the isothermal crystallization of PGA via THz, IR spectroscopy and simultaneous WAXD/SAXS measurements. We attempted to analyze the effects of intermolecular interactions on the development of the crystalline structure of PGA.

Materials and methods

Materials

PGA, with a melting point (T_m) of 217 °C and a glass transition temperature (T_g) of approximately 35–40 °C, was purchased from BMG Corp. (Japan). IR measurements for PGA were conducted for films with a thickness of ca. 20 μm obtained by casting a 1 wt% 1,1,1,3,3,3-hexafluoro-2-propanol solution on CaF_2 windows. The films were maintained at 60 °C in a vacuum-dried oven for 8 h, and then cooled down to room temperature. THz spectra measurements were conducted for films with a PGA thickness of ca. 200 μm prepared by melting onto Si windows. The PGA film sample for SAXS/WAXD measurements was prepared by hot pressing above its T_m, followed by rapid cooling of the film in air down to room temperature. The film was sealed between polyimide films each having a thickness of approximately 1 mm. The as-prepared samples were utilized for the isothermal crystallization measurements with SAXS and WAXD using the FSBL03XU beamline at SPring-8.

IR measurements

The transmission IR spectra were collected at a spectral resolution of 2 cm^{-1} using a Thermo Fisher Scientific Nicolet 6700 Fourier transform IR spectrometer equipped with a liquid-nitrogen-cooled mercury-cadmium-telluride (MCT) detector. To obtain a high signal-to-noise ratio, 128 scans for the isothermal crystallization process were co-added for each IR spectral measurement. The temperature of the sample cell that holds the CaF_2 window with PGA film was controlled using a Linkam controller 10002 L (Linkam Scientific Instruments Ltd., UK).

THz spectra measurements

A Fourier transform far-infrared (FT-FIR) spectrometer (JASCO FARIS) with a superconducting bolometer (QMC: QNbB/PTC) was employed for THz spectrum measurements. A total of 100 scans were accumulated in 5 min to obtain a single spectrum with a spectral resolution of 2 cm^{-1}. A film sample was placed onto the high-resistive Si window of the heating stage (Linkam 10002 L), with the temperature of the sample monitored using a K-type thermocouple attached to the sample. The heating stage was set in the FT-FIR measurement chamber, which was purged by a continuous flow of nitrogen gas to reduce the absorption of water vapor. In this study, the spectrum for the Si window was collected at room temperature before each sample measurement and employed as a reference for calculation of the absorption spectra.

For THz spectral measurement of the isothermal melt-crystallization process, once the sample was molten at 230 °C, it was rapidly cooled to 185 °C, with this temperature maintained for 120 min, at which point the THz spectra for the sample were continuously measured at an interval of 80 s.

SAXS/WAXD simultaneous measurements

The SAXS/WAXD data were collected for the as-prepared PGA sample with a wavelength of $\lambda = 1.0$ Å in the BL03XU beamline [24] at SPring-8, Harima, Japan. The distances between the sample and detector for the SAXS and WAXD measurements were set to be 1246 and 64 mm, respectively. The two-dimensional SAXS and WAXD patterns were simultaneously recorded every 6 s with an exposure time of 3 s using a CCD camera (Hamamatsu Photonics, Shizuoka, Japan, V7739P + ORCA R2) and an imaging plate (IP) system (Rigaku, Tokyo, Japan, RAXIS VII), respectively. The isothermal crystallization experiments were carried out at 185 °C with temperature fluctuations of less than ± 0.5 °C. A homemade temperature enclosure with two heating chambers was used for the temperature jump from 230 °C (above T_m) to 185 °C.

2D correlation analysis

In this study, a 2D-COS analysis was used to obtain more detailed information regarding the SAXS/WAXD profile and spectral variations observed during the isothermal crystallization process. The 2D-COS has two advantages: spectral resolution enhancement, and investigation of the sequential order of spectral variations. Furthermore, 2D-COS can highlight small spectral variations and demonstrate the relation between the bands. The 2D-COS technique creates a pair of synchronous $\Phi(\nu_1, \nu_2)$ and asynchronous $\Psi(\nu_1, \nu_2)$ 2D correlation spectra, where the spectral variables ν_1 and ν_2 are wavenumbers. The 2D-COS calculations were conducted using the 2D-Shige software (Kwansei Gakuin University, Japan).

Results and discussion

IR spectra

Time-dependent IR spectra in the regions of (a) 3000–2900 cm^{-1} (CH_2 stretching), (b) 1900–1600 cm^{-1} (C = O stretching), and (c)1500–1100 cm^{-1} obtained during the isothermal crystallization of a PGA cast film at 185 °C are shown in Fig. 2. In our previous temperature-dependent IR study of PGA, a band at 1245 cm^{-1} due to the C-O-C antisymmetric stretching mode suggested the existence of intermolecular hydrogen bonding between the CH_2 group and the ether oxygen atom of PGA in the crystalline structure [9].

We observed that the C-O-C and CH_2 bands showed similar thermal behavior, whereas the C = O band exhibited significantly different behavior during the heating process compared to the other bands [9]. During the isothermal crystallization process, the 1245 cm^{-1} band appeared at 240 s, with the band at 2959 cm^{-1}, originating from the CH_2 antisymmetric stretching, shifting to a higher wavenumber, while the band at 1741 cm^{-1}, due to the C = O stretching mode, appearing at 600 s. Since the band due to the C-O-C antisymmetric stretching mode and that arising from the CH_2 stretching mode demonstrate similar behavior during the isothermal crystallization process, weak hydrogen bonding may exist between the O atom of the C-O-C group and the H atom of the CH_2 group.

THz spectra

Figure 3 shows the THz absorption spectra measured during the isothermal melt-crystallization of PGA at 185 °C for 120 min. In Fig. 3, it is clearly seen that the crystalline bands for PGA at 65, 192, and 220 cm^{-1} show an increase in intensity, while the amorphous band at 97 cm^{-1} shows an intensity decrease [16]. In our previous study, the orientation of the vibrational dipole moment of these bands were obtained via polarized THz absorption spectra. The bands at 65 and 192 cm^{-1} are assigned to the vibrational modes perpendicular to the ***c***-axis of the lamellar crystal, while the band at 220 cm^{-1} is assigned to the vibrational modes parallel to the *c*-axis.

Figure 4 shows the intensity variations of the band at 65 cm^{-1} and 192 cm^{-1}, respectively, during the isothermal melt-crystallization at 185 °C. A significant difference is observed between these two plots for the starting time of the intensity change. The absorption intensity at 192 cm^{-1} starts increasing at 1200 s, with the absorption at 65 cm^{-1} starting to increase after 1800 s. Similar phenomena were observed in our previous studies of PHB [13]. During the isothermal crystallization of PHB, the perpendicular band originating from the vibration of C = O···H-C hydrogen bonds (72 cm^{-1}) initially increased, and, subsequently, the band intensity for the skeletal motion parallel to the *c*-axis (97 cm^{-1}) increased [13]. We elucidated these differences via two-step crystal formation, where first the hydrogen bonding network is constructed, and then, the crystal grows along the *c*-axis. However, in this study, the difference in the intensity change is observed between two bands having the same direction for the vibrational motion, which is perpendicular to the *c*-axis. Therefore, we should consider more details regarding the difference in the vibrational motion.

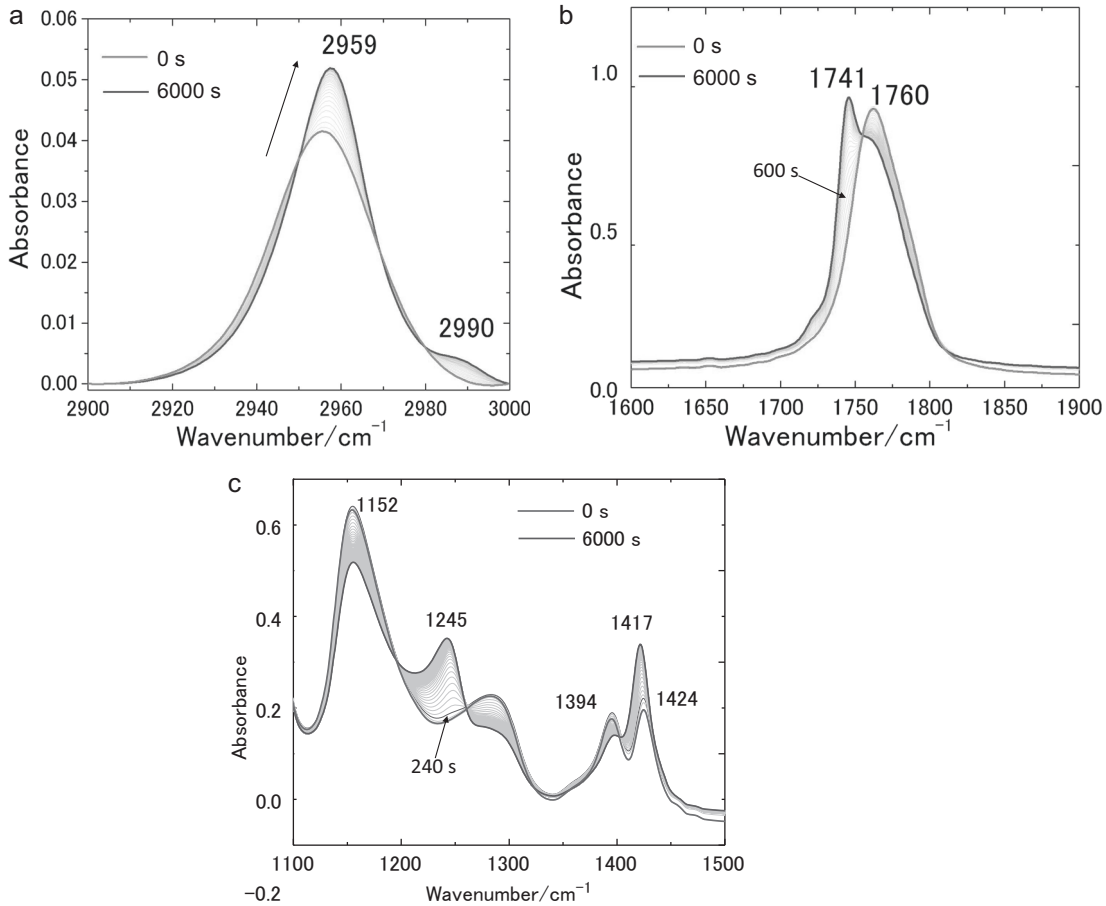

Fig. 2 **a** Time-dependent IR spectra in the region of 3000–2900 cm^{-1} collected during the melt-crystallization process of PGA at 185 °C. **b** Time-dependent IR spectra in the region of 1900–1600 cm^{-1} collected during the melt-crystallization process of PGA at 185 °C. **c** Time-dependent IR spectra in the region of 1500–1100 cm^{-1} collected during the melt-crystallization process of PGA at 185 °C

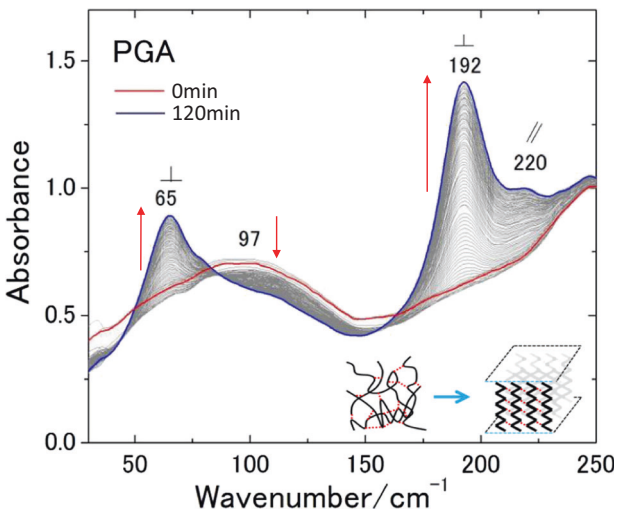

Fig. 3 Time-dependent terahertz absorption spectra collected during the melt-crystallization process of PGA at 185 °C

In general, vibrational motion appearing in the THz and FIR region is a mixed motion composed of inter- and intramolecular vibrations. As the vibrational frequency becomes lower, the intermolecular vibrations become dominant, with intramolecular vibration becoming the primary origin for the absorption bands at higher frequency [25]. The bands at 65 and 192 cm^{-1} both exhibit the perpendicular vibrational mode with respect to the *c*-axis, but the contributions of inter- and intramolecular motions are different in these two bands.

The band at 65 cm^{-1} originates dominantly from the out-of-plane bending vibration of the C = O group that oscillates concurrently with the C atoms in the backbone [16]. The center frequency of this band exhibits a redshift when the sample is heated, due to the thermal expansion of the crystalline lattice [16]. Therefore, this vibrational mode is sensitive to the change in the interchain distance of the crystalline PGA. Furthermore, the band at 192 cm^{-1} was attributed to rocking/twisting of CH_2 coupled with the deformation of the bond O-CH_2, and does not indicate temperature shifting [16]. The CH_2 rocking/O-CH_2 deformation mode of the molecular chain of PGA was primarily ascribed to the twisting of the local structure of the PGA molecular chain. Therefore, the vibrational mode of this

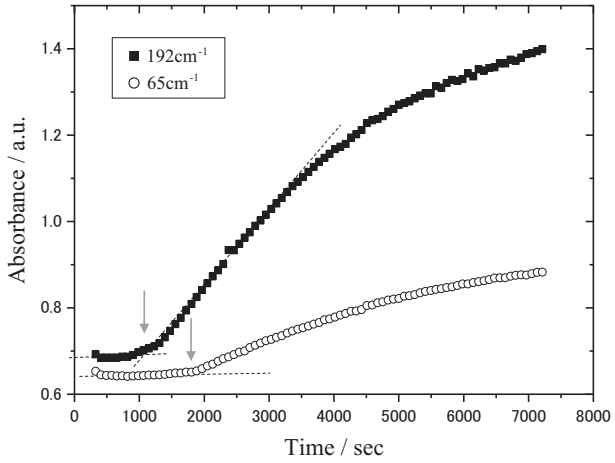

Fig. 4 Variations of intensity for the absorption peaks observed in the terahertz (THz) region as a function of time during the isothermal melt-crystallization process at 185 °C

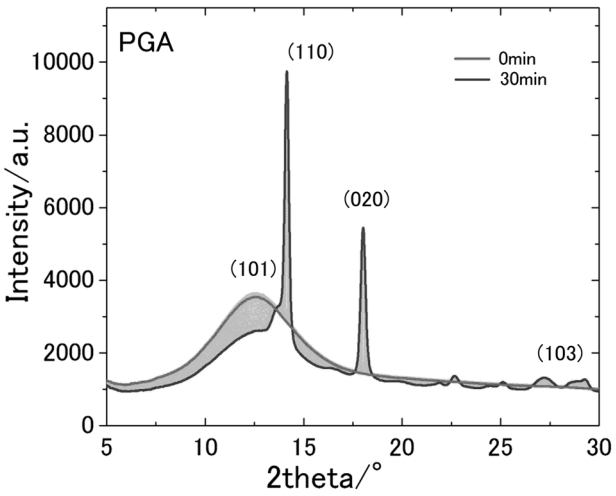

Fig. 5 Time-dependent WAXD profile measured during the isothermal melt-crystallization process of PGA at 185 °C

band is primarily dependent on the deformation of the intrachain mode.

The temporal difference in the intensity observed in the isothermal crystallization is due to the difference of the vibrational origins of these two bands. The band at 192 cm^{-1}, primarily originating from the intramolecular vibrational mode, starts increasing at 1200 s, when the polymer chain forms a disordered crystalline PGA structure. The band at 192 cm^{-1} is due to the intramolecular vibrational mode (twisting of the local structure of the PGA molecular chain); however, it is necessary that a molecular chain that is arranged regularly to some extent is formed. Furthermore, the band at 65 cm^{-1} increases after 1800 s due to the formation of the C = O···H-C hydrogen bonds between the polymer chains. Since the growth of the band at 65 cm^{-1} (intramolecular vibrational mode) appears together with the formation of the ordered crystal structure, it is necessary that the molecular chains in the crystal lamellae are sufficiently close to each other. Hence, the temporal difference in the intensity of these two bands can be thought of as the difference in the formation between the short-range order and the long-range order.

SAXS/WAXD measurements

Figure 5 shows the WAXD profile obtained during the isothermal melt-crystallization process for PGA at 185 °C for 30 min. In Fig. 5, the peaks at $2\theta \cong 14.2°$ and 18.1° exist due to the (110) and (020) diffractions from the PGA crystals. As mentioned above, PGA has an orthorhombic, $Pcmn - D_{2h}^{16}$ unit cell with lattice parameters $a = 5.22$ Å, $b = 6.19$ Å, and $c = 7.02$ Å [3]. The time dependence for the (110) and (020) lattice spacing was estimated by using the results shown in Fig. 5. Figure 6 plots the time dependence, $d(t)/d(\infty)$, for the (110) and (020) diffraction peaks. Here, $d(\infty)$ indicates the lattice spacing of the (110) and (020) diffractions at $t = 1800$ s. It can be clearly seen from Fig. 6 that the lattice spacing for (110) converges at approximately 306 s. Moreover, in the case of the (020) diffraction, the lattice spacing for (020) converges at approximately 1098 s. Our previous studies have indicated that weak C-H···O (ether) hydrogen bonding exists along the (110) direction in PGA [9]. Therefore, it is highly possible that intermolecular interactions control the structural formation of the crystalline structure of PGA in the early stage of the isothermal crystallization process. Furthermore, 2D correlation analysis was employed to better understand the formation of the crystal structure in PGA using a time-dependent WAXD profile.

To analyze the sequential order of the intensity variations for the diffraction peaks during the isothermal melt-crystallization process of PGA, we used 2D-COS analysis. The 2D-COS analysis is a useful technique to provide a better understanding of investigated phenomena even in the case of complicated spectral intensity variations for highly overlapped bands [20–22]. The 2D correlation spectra for PGA between the (110) and (020) diffraction regions were constructed based on time-dependent WAXD profiles obtained during the isothermal crystallization process from t = 6 to 366 s at 185 °C. Figure 7a, b show the synchronous and asynchronous 2D correlation spectra, respectively. In the synchronous 2D correlation spectrum (Fig. 7a), a positive cross peak is observed at $2\theta = 14.15°$ ((110) diffraction) and $2\theta = 18.05°$ ((020) diffraction), while other regions show a negative peak.

The 2D-COS results indicate that the (110) and (020) diffraction peaks increase in intensity. Furthermore, the cross peak at (14.15, 18.05) shows a positive sign in the asynchronous 2D correlation spectrum (Fig. 7b). It should be noted that the (110) diffraction peak increases faster than

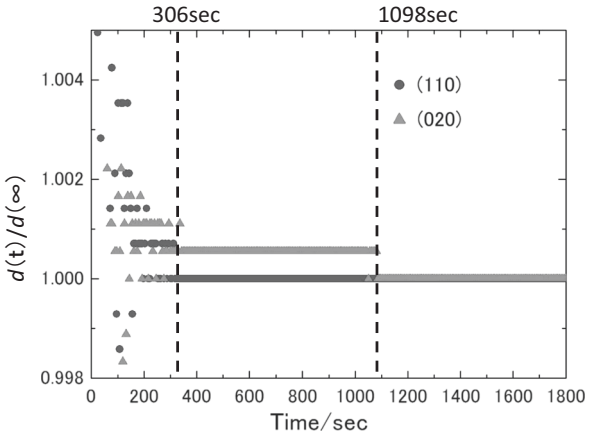

Fig. 6 A time evolution of the ratio of the d-spacing $d(t)/d(\infty)$ during the isothermal melt-crystallization process in PGA at 185 °C

the (020) diffraction peak during the isothermal crystallization of PGA.

Figure 8 shows the time-resolved Lorentz-corrected SAXS profiles obtained for PGA during isothermal crystallization at 185 °C for 30 min. It was observed that a scattering peak appeared after 366 s, which indicates that the peak widths of the (110) and (020) diffraction peaks converged in the time-resolved WAXD profile (Fig. 5). In addition, a scattering peak was shifted to a large q value ($\sim 0.45\ nm^{-1}$) with time. The time evolution of the characteristic parameters (long period $L(t)$, lamellar-crystal thickness $l_{cry}(t)$, amorphous layer thickness $l_{amo}(t)$, and scattering invariant $Q(t)$) were estimated using one-dimensional correlation analysis from the Lorentz-corrected SAXS profiles (Fig. 8). The results are shown in Fig. 9. After the induction period of $t_0 \sim 200$ s, the invariant $Q(t)$ starts to increase sigmoidally with time. We note that the (110) diffraction peak reached an almost constant value at t ~306 s, while the value for the invariant $Q(t)$ had not yet started to increase at this time. This result also indicates that the weak C-H···O (ether) hydrogen bonding that exists along the (110) direction in PGA appears in the microcrystals of PGA during the early stage of the crystallization process.

Figure 10a, b show the synchronous $\Phi(\nu_1,\nu_2)$ and asynchronous $\Psi(\nu_1,\nu_2)$ 2D correlation spectra, respectively, based on the SAXS profile changes in the q range 0.2–1.2 nm^{-1} during the isothermal crystallization process from t = 366 to t = 846 s at 185 °C. The 2D correlation map shows that $\Phi(0.3, 0.45) > 0$ and $\Psi(0.3, 0.45) > 0$, $\Phi(0.7, 0.45) > 0$, and $\Psi(0.7, 0.45) > 0$. These results indicate that the peak intensities at $q = 0.3$ and 0.7 nm^{-1} changed faster than the peak intensity at $q = 0.45\ nm^{-1}$. The peaks at $q = 0.3$ and 0.7 nm^{-1} may exist due to the density fluctuation in a homogeneous matrix of the amorphous state, since the 2D-COS analysis was

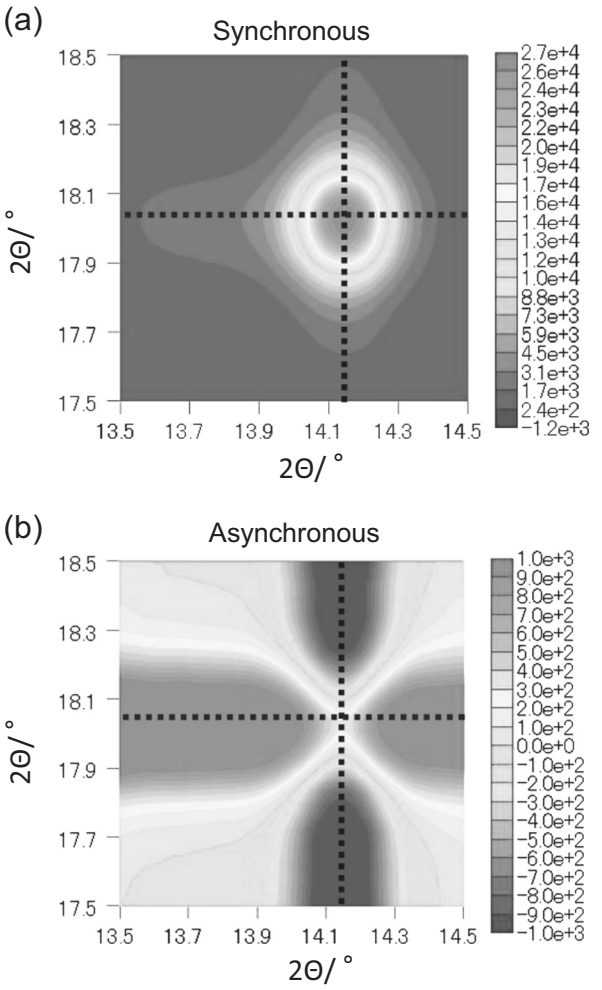

Fig. 7 **a** Synchronous and **b** asynchronous correlation maps calculated from the WAXD profiles obtained during the melt-crystallization process in PGA at 185 °C

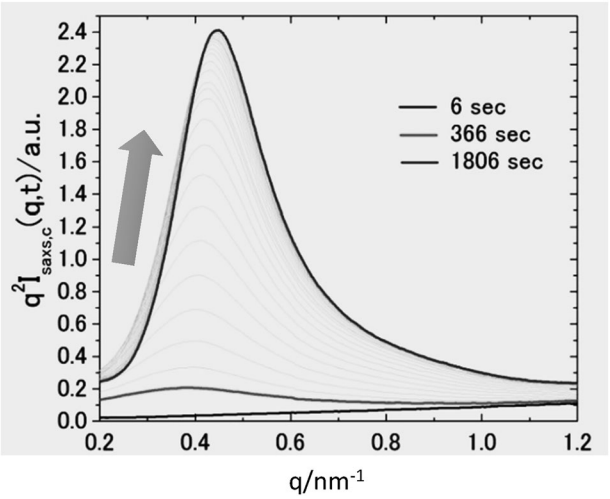

Fig. 8 Lorentz-corrected SAXS profiles for PGA obtained during the isothermal melt-crystallization process at 185 °C

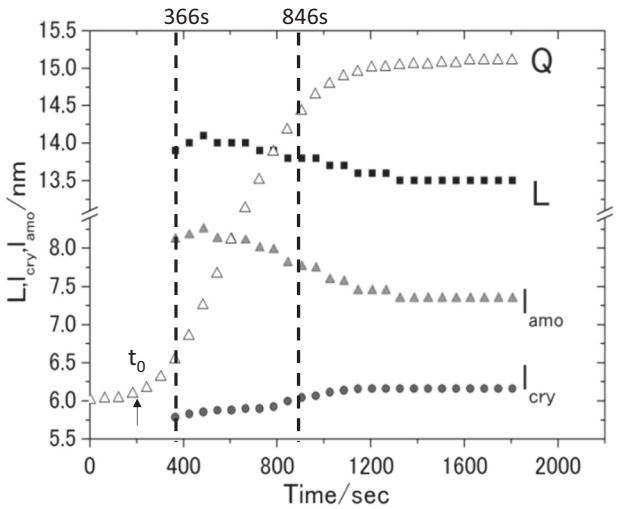

Fig. 9 Variations of characteristic parameters obtained from the one-dimensional correlation function such as the long period L, lamellar-crystal thickness l_{cry}, amorphous layer thickness l_{amo}, and invariant Q as a function of time during the isothermal melt-crystallization process at 185 °C

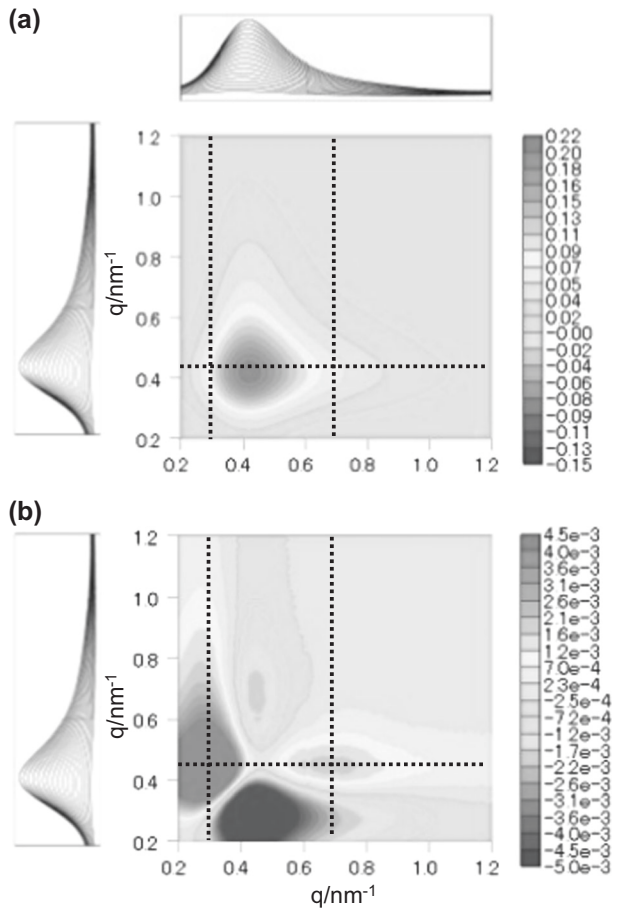

Fig. 10 **a** Synchronous and **b** asynchronous correlation maps calculated from the SAXS profiles obtained during the melt-crystallization process in PGA at 185 °C

conducted in the early and intermediate stages of the isothermal crystallization process. From 2D-COS analysis, it can be observed that the density fluctuations formed faster than the lamellar crystal ($q = 0.45\,nm^{-1}$). The SAXS and WAXD investigations of the crystallization process of PGA have suggested the following conclusions: first, the microcrystal appears, and then, the density fluctuations are built up, with the lamellar crystallites finally appearing during the isothermal crystallization process.

The above results from the THz and SAXS/WAXD measurements taken during the isothermal crystallization of PGA demonstrate that the crystallization of PGA may be triggered by the weak hydrogen bonding between two parallel molecular chains in the PGA crystallites. In addition, THz absorption crystalline peaks appeared after the development of the peaks in the SAXS and WAXD profiles of PGA. Since the SAXS/WAXD measurements and the THz spectra are not simultaneous measurements, the time axis does not completely satisfy the X-ray and THz experiments. However, an interesting result is that the absorption crystalline peaks in the THz data appeared after the appearance of the SAXS/WAXD peaks due to the crystalline structure. The onset of the intensity change for the peak at 192 cm^{-1} in the THz spectra is almost in agreement with the time when the invariant Q becomes a constant value. Most likely, the intermolecular vibration appearing in the THz spectra requires the molecular chains to be oriented. Therefore, it is highly possible that the THz absorption peaks at 192 and 65 cm^{-1} appear after the formation of the crystal lamellae.

Conclusion

In this work, we have studied the isothermal crystallization of PGA using THz and IR spectroscopy and simultaneous SAXS/WAXD measurements; in addition, we have conducted 2D-COS analysis to resolve the sequential order of the peaks observed in the SAXS and WAXD profiles for PGA during the isothermal crystallization. From the THz spectral results, we observed that the intensity of the absorption peak at 192 cm^{-1} increased before the increase in intensity of the peak at 65 cm^{-1} during the isothermal melt-crystallization process at 185 °C. The band at 192 cm^{-1} primarily originates from the intramolecular vibrational mode. Moreover, the band at 65 cm^{-1} exists due to the C = O···H-C hydrogen bonds between the polymer chains. The temporal difference in the intensity observed in the isothermal crystallization is due to the difference in the vibrational origins of these two bands.

The results from the simultaneous SAXS/WAXD measurements indicated that the weak C-H···O (ether)

hydrogen bonding that exists along the (110) direction in PGA appears in PGA microcrystals during the early stage of the crystallization process. The absorption crystalline peaks in the THz spectra appeared after the appearance of the SAXS and WAXD peaks due to the crystalline structure. It is highly possible that the intermolecular vibration appearing in the THz spectra requires the molecular chains to be oriented. Comparing THz and simultaneous SAXS/WAXD measurements, it can be observed that the disordered crystalline structure in PGA developed first, before the formation of C-H···O (ether) intermolecular interactions; then, finally, the ordered lamellar crystallites were developed. The SAXS/WAXD profile and THz spectra indicated that the hydrogen bonding in PGA dominates crystallization in the early stage of the isothermal crystallization process. Therefore, it may be concluded that the C-H···O hydrogen bond between the H atom of the CH_2 group and the O atom of the ether group controls the crystallization of PGA. Presumably, the intermolecular interactions affect the higher-order structure of PGA.

Acknowledgements This work was supported by the Industry–Academia Collaborative R&D from the Japan Science and Technology Agency, JST. Synchrotron radiation experiments were performed at the FSBL03XU of SPring-8 in collaboration with the Japan Synchrotron Radiation Research Institute (JASRI).

Compliance with ethical standards

Conflict of interest The authors declare no conflicts of interest associated with this manuscript.

References

1. Carothers WH, Dorough GL, Van Natta FJ. Studies of polymerization and ring formation. X. The reversible polymerization of six-membered cyclic esters. J Am Chem Soc. 1932;54:761–72. https://doi.org/10.1021/ja01341a046
2. Montes de Oca H, Ward IM, Chivers RA, Farrar DF. Structure development during crystallization and solid-state processing of poly(glycolic acid). J Appl Polym Sci. 2008;111:1013–8. https://doi.org/10.1002/app.29000
3. Chatani Y, Suehiro K, Okita Y, Tadokoro H, Chujo K. Structural studies of polyesters. I. Crystal structure of polyglycolide. Die Makromol Chem. 1968;113:215–29. https://doi.org/10.1002/macp.1968.021130119
4. Tadokoro H, Kobayashi M, Yoshidome H, Tai K, Makino D. Structural Studies of Polyesters. II. Far-Infrared Spectra of Aliphatic Polyesters: Comparison with Polyamides. J Chem Phys. 1968;49:3359–3373. https://doi.org/10.1063/1.1670608
5. Kister G, Cassanas G, Vert M. Morphology of poly(glycolic acid) by IR and Raman spectroscopies. Spectrochim Acta Part A. 1997;53:1399–403. https://doi.org/10.1016/S0584-8539(97)00039-1
6. Schmitt EE, Polistina RA US Pat. 3, 033 (1967).
7. Shiiki, Z; Kawakami, Y, US Pat. 5, 991 (1998).
8. Lowe, CE, US Pat. 2, 162 (1954).
9. Sato H, Miyada M, Yamamoto S, ReddyK R, Ozaki Y. C–H···O (ether) hydrogen bonding along the (110) direction in polyglycolic acid studied by infrared spectroscopy, wide-angle X-ray diffraction, quantum chemical calculations and natural bond orbital calculations. RSC Adv. 2016;6:16817–23. https://doi.org/10.1039/c5ra19900j
10. Fuse N, Sato R, Mizuno M, Fukunaga K, Itoh K, Ohki Y. Observation and analysis of molecular vibration modes in polylactide at terahertz frequencies. Jpn J Appl Phys. 2010;49:102402 https://doi.org/10.1143/JJAP.49.102402
11. Hoshina H, Morisawa Y, Sato H, Minamide H, Noda I, Ozaki Y, et al. Polarization and temperature dependent spectra of poly(3-hydroxyalkanoate)s measured at terahertz frequencies. Phys Chem Chem Phys. 2011;13:9173–9. https://doi.org/10.1039/C0CP02435J
12. Hoshina H, Morisawa Y, Sato H, Kamiya A, Noda I, Ozaki Y, et al. Higher order conformation of poly(3-hydroxyalkanoates) studied by terahertz time-domain spectroscopy. Appl Phys Lett. 2010;96:101904. https://doi.org/10.1063/1.3358146
13. Hoshina H, Ishii S, Morisawa Y, Sato H, Noda I, Ozaki Y, et al. Isothermal crystallization of poly(3-hydroxybutyrate) studied by terahertz two-dimensional correlation spectroscopy. Appl Phys Lett. 2012;100:011907. https://doi.org/10.1063/1.3673847
14. Funaki C, Toyouchi T, Hoshina H, Ozaki Y, Sato H. Terahertz Imaging of the Distribution of Crystallinity and Crystalline Orientation in a Poly(ε-caprolactone) Film. Appl Spectrosc. 2017;7:1537–42. https://doi.org/10.1177/0003702816684838
15. Yamamoto S, Morisawa Y, Sato H, Hoshina H, Ozaki Y. Quantum mechanical interpretation of intermolecular vibrational modes of crystalline poly-(R)-3-hydroxybutyrate observed in low-frequency raman and terahertz spectra. J Phys Chem B. 2013;117:2180–7. https://doi.org/10.1021/jp309704k
16. Yamamoto S, Miyada M, Sato H, Hoshina H, Ozaki Y. Low-frequency vibrational modes of poly(glycolic acid) and thermal expansion of crystal lattice assigned on the basis of DFT-spectral simulation aided with a fragment method. J Phys Chem B. 2017;121:1128–38. https://doi.org/10.1021/acs.jpcb.6b11304
17. Zhang F, Wang HW, Tominaga K, Hayashi M, Lee S, Nishino T. Elucidation of chiral symmetry breaking in a racemic polymer system with terahertz vibrational spectroscopy and crystal orbital density functional theory. J Phys Chem Lett. 2016;7:4671–6. https://doi.org/10.1021/acs.jpclett.6b02213
18. Zhang F, Wang HW, Tominaga K, Hayashi M. Mixing of intermolecular and intramolecular vibrations in optical phonon modes: terahertz spectroscopy and solid-state density functional theory. WIREs Comput Mol Sci. 2016;6:386–409. https://doi.org/10.1002/wcms.1256
19. Zhang F, Wang HW, Tominaga K, Hayashi M. Characteristics of low-frequency molecular phonon modes studied by thz spectroscopy and solid-state ab initio theory: polymorphs I and III of diflunisal. J Phys Chem B. 2016;120:1698–710. https://doi.org/10.1021/acs.jpcb.5b08798
20. Noda I. Generalized two-dimensional correlation method applicable to infrared, Raman, and other Types of spectroscopy. Appl Spectrosc. 1993;47:1329–36. https://doi.org/10.1366/0003702934067694
21. Noda I, Dowrey AE, Marcott C, Story GM, Ozaki Y. Generalized two-dimensional correlation spectroscopy. Appl Spectrosc. 2000;54:236–48. https://doi.org/10.1366/0003702001950454
22. Noda I, Ozaki Y. Two-dimensional Correlation. Spectroscopy - Applications in Vibrational and Optical Spectroscopy. Chichester, West Sussex: John Wiley & Sons; 2004. ISBN978-0-471-62391-5
23. Guo L, Sato H, Hashimoto T, Ozaki Y. Thermally induced exchanges of hydrogen bonding interactions and their effects on phase structures of poly(3-hydroxybutyrate) and poly(4-

vinylphenol) blends. Macromolecules. 2011;44:2229–39. https://doi.org/10.1021/ma102601p
24. Masunaga H, Ogawa H, Takano T, Sasaki S, Goto S, Tanaka T, et al. Multipurpose soft-material SAXS/WAXS/GISAXS beamline at SPring-8. Polym J. 2011;43:471–7. https://doi.org/10.1038/pj.2011.18
25. Zhang F, Wang HW, Tominaga K, Hayashi M. 2016. Mixing of intermolecular and intramolecular vibrations in optical phonon modes: terahertz spectroscopy and solid-state density functional theory. Comput Mol Sci. 2016;6:386–409. https://doi.org/10.1002/wcms.1256